A 3D numerical simulation of stress distribution and fracture process in a zirconia-based FPD framework

Wen Kou,[1] Decong Li,[2] Jiyan Qiao,[2] Li Chen,[2] Yansheng Ding,[2] Göran Sjögren[1]

[1]Department of Dental Materials Science, Faculty of Medicine, Umeå University, Umeå SE-901 87, Sweden
[2]Institute of Mechanics, Chinese Academy of Sciences, Beijing CN-100190, China

Received 2 April 2010; revised 5 September 2010; accepted 25 October 2010
Published online 28 December 2010 in Wiley Online Library (wileyonlinelibrary.com). DOI: 10.1002/jbm.b.31782

Abstract: In this study, a numerical approach to the fracture behavior in a three-unit zirconia-based fixed partial denture (FPD) framework was made under mechanical loading using a newly developed three-dimensional (3D) numerical modeling code. All the materials studied were treated heterogeneously and Weibull distribution law was applied to describe the heterogeneity. The Mohr-Coulomb failure criterion with tensile strength cut-off was utilized to judge whether the material was in an elastic or failed state. For validation, the fracture pattern obtained from the numerical modeling was compared with a laboratory test; they largely correlated with each other. Similar fracture initiation sites were detected both in the numerical simulation and in an earlier fractographic analysis. The numerical simulation applied in this study clearly described the stress distribution and fracture process of zirconia-based FPD frameworks, information that could not be gained from the laboratory tests alone. Thus, the newly developed 3D numerical modeling code seems to be an efficient tool for prediction of the fracture process in ceramic FPD frameworks. © 2010 Wiley Periodicals, Inc. J Biomed Mater Res Part B: Appl Biomater 96B: 376–385, 2011.

Key Words: ceramics, finite element analysis, fixed partial denture, fracture process, numerical simulation

INTRODUCTION

Ceramics have long been used as a material for dental restorations, mainly because of their good aesthetic qualities, biocompatibility, chemical inertness,[1] and resistance to wear.[2] During the last few decades, the introduction of ceramics with improved mechanical properties has resulted in increased use of all-ceramic fixed partial dentures (FPDs), even in the posterior region of the oral cavity.[3,4] The so-called oxide ceramics, based on densely sintered alumina or yttria stabilized tetragonal zirconia polycrystals (Y-TZP) are examples of recently introduced ceramics with improved properties.[4–6] These ceramics have excellent properties and zirconia in particular has better flexural strength and fracture resistance than other dental ceramics.[7,8] Recently published follow-up studies of zirconia-based all-ceramic FPDs have also produced promising results.[9–12]

However, one remaining problem with ceramic materials is their brittleness. Brittle fracture is a fracture phenomenon that frequently occurs in ceramics, and the fracture behavior differs from that seen in ductile materials, such as metals. In a brittle fracture, no or little apparent plastic deformation takes place before fracture, and once a fracture is initiated, it often propagates rapidly, leading ultimately to total catastrophic failure.[13] It is, therefore, of particular interest to study stress distribution, fracture initiation and propagation in ceramics in order to gain further knowledge about the fracture process and to determine how to prolong the lifetime of ceramic constructions.

Today there are a number of techniques available for studying fracture in materials[13]; one frequently applied method is the fractographic analysis method,[14–16] which often allows the fracture mechanism to be interpreted and the fracture initiation to be localized.[13,16] However, fractographic analysis can only be applied once the specimen has fractured and cannot identify the stress distribution and fracture propagation during the fracture process. Since the laboratory tests are often destructive, relatively expensive and unable to show stress distribution and the fracture process clearly, it is worthwhile developing other methods for analyzing stress distribution and fracture behavior in ceramic materials. The numerical method is one such method which has been used to analyze physical phenomena in the field of solid and fluid mechanics problems, among others, and has been employed in a variety of areas such as biomechanics.[17–19] In an earlier study, a two dimensional (2D) numerical simulation code, the R-T^{2D} code, was applied in an analysis of the fracture mechanism and process in a three-unit FPD framework made of hot isostatic pressed (HIPed) Y-TZP placed on stainless steel abutments.[20] The results showed that the fracture process obtained by using this R-T^{2D} code correlated fairly well with a previous laboratory study of a three-unit HIPed Y-TZP FPD framework.[20]

Correspondence to: W. Kou; e-mail: wen.kou@odont.umu.se
Contract grant sponsors: Faculty of Medicine, Umeå University, Umeå, Sweden; The Swedish Society for Medical Research; The Kempe Foundation, and The Wallenberg Foundation

However, since the loading conditions and the stress distribution in the oral cavity are complex, three-dimensional (3D) numerical modeling would provide more information about the stress distributions and fracture processes in all-ceramic FPDs.[20] Moreover, since previous studies have shown that machining ceramic restorations produces grooves, often described as milling trace lines, on the surface of ceramic frameworks[16,21] and that manual grinding may introduce irregularities on ceramic surfaces,[22] it is of interest to examine how such grooves/irregularities on the ceramic surfaces affect the fracture process.

Although the reliability of all-ceramic dental prosthesis systems has been studied in earlier papers,[23,24] a survey of the literature revealed no article that clearly showed the fracture process of all-ceramic FPDs using a 3D numerical modeling code, which took into consideration the heterogeneity of the material. In addition, no article was found that evaluated the way in which irregularities, such as grooves, on the ceramic surfaces, affect the fracture of ceramic FPD frameworks using a 3D numerical modeling code. The aim of the present study was therefore: (i) to examine the stress distribution and fracture process in a three-unit ceramic FPD framework under simulated mechanical loading; (ii) to validate the numerical simulation results against a laboratory test; and (iii) to investigate the effect of surface grooves/irregularities introduced on the fracture of a ceramic FPD framework using a newly developed 3D numerical modeling code, which considers the material's heterogeneity.

MATERIALS AND METHODS

Laboratory test

One specimen of a three-unit HIPed Y-TZP FPD framework, which had been CAD/CAM (computer aided designing/computer aided manufacturing) fabricated (Cad.esthetics AB, Skellefteå, Sweden) was used as the base for the size and geometric form of the framework studied in the present numerical simulation [Figure 1(a–c)]. The size and geometric design of this framework was identical to the frameworks tested in an earlier fractographic study.[16] The distance between the centers of the abutments was 17.5 mm and the size of the cross-section of the connecting area between the retainer and the pontic was 3 mm × 3 mm. After the framework was cemented, using zinc phosphate cement (PhosphatCEM IC, Vivadent/Ivoclar, Schaan, Liechtenstein), on to stainless steel abutments in a stainless steel socket the specimen was static loaded, occlusally, until fracture occurred, using a universal testing machine (Tinius Olsen H10K-T, Horsham, PA).

Numerical simulation

Mathematical description of the heterogeneity of material properties. All the materials used in the present simulation were assumed to be mesoscopically heterogeneous. Mesoscopic heterogeneity means that the media are presented uniformly and isotropically in a mesoscopic element but heterogeneously among different elements.

In this study, the Weibull distribution law[25] was utilized to assign the values of the element parameters to give the elements varying mechanical properties. The Weibull distribution law is described in the following formula:

$$\varphi(\sigma) = \begin{cases} \frac{m}{\sigma_0}\left(\frac{\sigma}{\sigma_0}\right)^{m-1} \exp\left[-\left(\frac{\sigma}{\sigma_0}\right)^{m}\right], \sigma \geq 0 \\ 0, \sigma < 0 \end{cases} \quad (1)$$

where $\varphi(\sigma)$ is the probability function of σ, σ is the element parameter which can be compressive strength, tensile strength, or Young's modulus of the element, σ_0 is the mean value of the element parameter and m is the Weibull modulus. The Weibull modulus is a homogeneous index of a material. A larger m implies a more homogeneous material and vice versa. When m trends to infinity, the variance of the value σ among the elements approaches zero, meaning that the material simulated becomes absolutely homogeneous. The specific heterogeneity distribution in 3D physical space after generation of finite elements was achieved by the Monte Carlo method.[26]

Mechanical model. As mentioned above, the material was considered homogeneous and isotropic in each individual element and heterogeneous among different elements. The relationship of elasticity between strain and stress observes Hooke's law. The stress equilibrium equation is applied and the effect of gravitational force is neglected.

The Mohr-Coulomb strength criterion with tensile strength cut-off was applied in judging whether the material was in an elastic state or had failed. The Mohr-Coulomb strength criterion is expressed as

$$|\tau_P| + \sigma_P \tan\phi - \tau_s \geq 0 \quad (2)$$

and the tensile strength cut-off is

$$\sigma_1 \geq \sigma_t \quad (3)$$

where τ_p is the shear stress and σ_p is the normal stress for one sectioned surface element through the point examined. In this study, tensile stress is assumed to be positive and, therefore, σ_1 is the maximum principal stress at that point. ϕ and τ_s are the friction angle and the shear strength of the material, respectively and σ_t is the uniaxial tensile strength of the material. The material will be in a state of failure if Eq. (2) and/or Eq. (3) are/is valid. Once the material fails the elastic modulus will degrade by a factor of R.

The geometric boundary of the three-unit zirconia-based framework with abutments is shown in Figure 1(d,e). The displacement load was applied on the occlusal surface of the simulated framework (Figure 2).

The relationships mentioned above, together with the boundary conditions, describe a complete mechanics problem for obtaining the deformation and fracture of the framework under loading. Numerical methods were resorted to in order to solve the problem. Detailed descriptions of the relationship between stress and strain and the Mohr-Coulomb strength criterion can be found in Jaeger and Cook.[27]

Numerical methods. The numerical simulation code used in the present study was developed at the Institute of Mechanics,

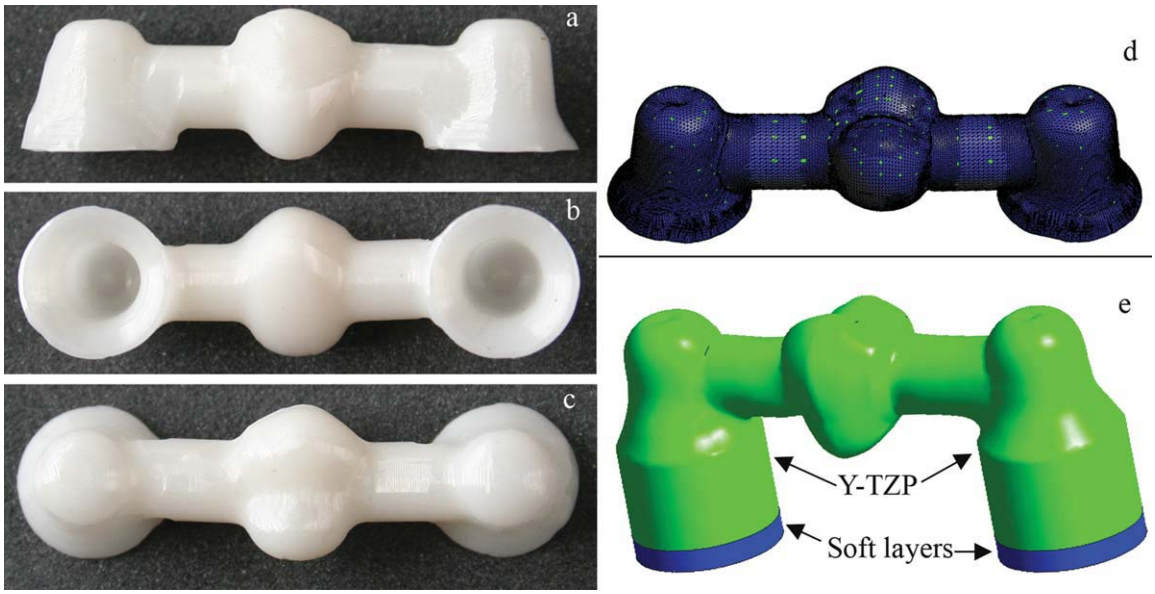

FIGURE 1. The shape of the three-unit HIPed Y-TZP framework before loading to fracture. (a) Buccal view. (b) Gingival view. (c) Occlusal view. The geometrical model used for the numerical simulation is shown in (d) and (e). (d) Lingual view of the three-unit framework from the CAD file. The location of the selected nodes on the geometric model is marked with the color green. (e) Buccal view of the three-unit framework. The green area is simulated as Y-TZP and the blue areas as the soft layers. [Color figure can be viewed in the online issue, which is available at wileyonlinelibrary.com.]

Chinese Academy of Sciences in Beijing, China. It is based on GiD (CIMNE, Barcelona, Spain), a 3D graphic preprocessor and postprocessor for computer simulation and Finite Element Program Generator (FEPG, Fegensoft, Beijing, China), which is a platform for generating finite element modeling codes. The FEPG is unique in that once the user writes partial differential equations and algorithm expressions for a problem, the FEPG can automatically generate a complete source code. The most important advantage of the numerical simulation code used in the present study is its suitability for simulating the fracture process in brittle and nonhomogeneous materials.

The geometric form of the framework in the laboratory test was designed by a CAD program. For the geometric shape in the numerical simulation, representative nodes were selected from the CAD data [Figure 1(d)] and the coordinates of the nodes were entered into GiD to generate finite elements for the solid model of the framework. In total 302,200 tetrahedral elements without mid-side nodes were generated. Two loading areas placed occlusally on the framework's pontic and shifted a little to the right abutment, similar to the laboratory test [Figure 2(a)], were created on the geometric model [Figure 2(b)]. Displacement of these two loading areas was then applied, 0.002 mm/step by step. The abutments were simulated as Y-TZP ceramic [Figure 1(e)] and soft layers were placed under the abutments [Figure 1(e)]. The Y-TZP ceramic and soft layers were assumed to be heterogeneous materials. Deformations of the abutments and the soft layers were also simulated. The displacement in the normal direction at the bottom surfaces of the soft layers was zero. The normal stress perpendicular and shear stress parallel to the boundary surface of the other parts of the framework were also zero. The mechanical properties of the materials used are listed in Table I.

To describe the progressive failure of the material a parameter named "flag" attached to each element was introduced. The definition of the flag is $\frac{N_f}{N}$, where N is the total number of the element nodes and N_f is those that failed. An element had completely failed when the flag $=$ 1 and was without any damage when the flag $=$ 0. An element was

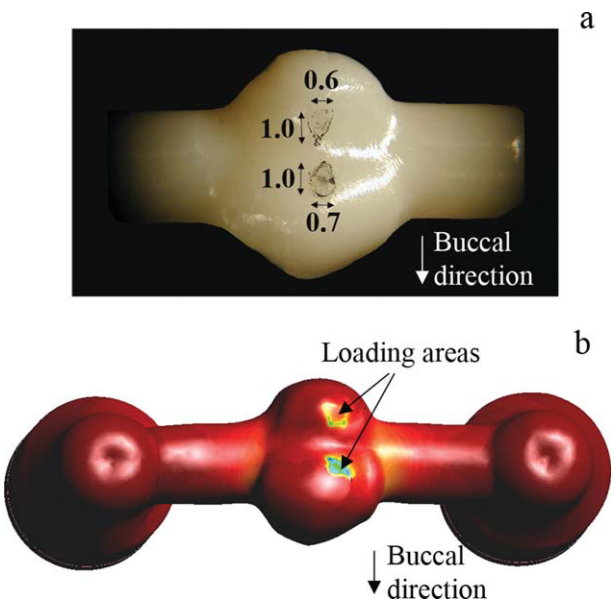

FIGURE 2. (a) Occlusal view of the pontic of the three-unit framework in the laboratory test. The loading areas are marked and the size of the loading areas is denoted in millimeters. (b) Occlusal view of the geometric model of the framework for the numerical simulation. The loading areas are marked with the color green. [Color figure can be viewed in the online issue, which is available at wileyonlinelibrary.com.]

TABLE I. The Parameters of the Materials used in the Present Numerical Simulation

Type of Material	Uniaxial Compressive Strength (MPa)	Tensile Strength (MPa)	Young's Modulus (GPa)	Weibull Modulus	Poisson's Ratio
Y-TZP	3500[a]	840 [28]	220 [28]	10 [29]	0.25[a]
Soft layer	22×10^4	84×10^4	22	10	0.26

[a] Manufacturer's information.
The numbers within square brackets [] denote the reference number.

partly damaged when 0<flag<1 and the increase of the flag from 0 to 1 describes the progressive failure of the element.

Introduction of grooves. To numerically simulate the effect of surface grooves/irregularities on fracture of the ceramic FPD framework, a cylinder-shaped zirconia-based bar was created with one groove introduced on the surface. The groove was located opposite the loading area and perpendicular to the central plane of the framework, where the highest tensile stress was expected [Figure 3(a)]. Two fixed support

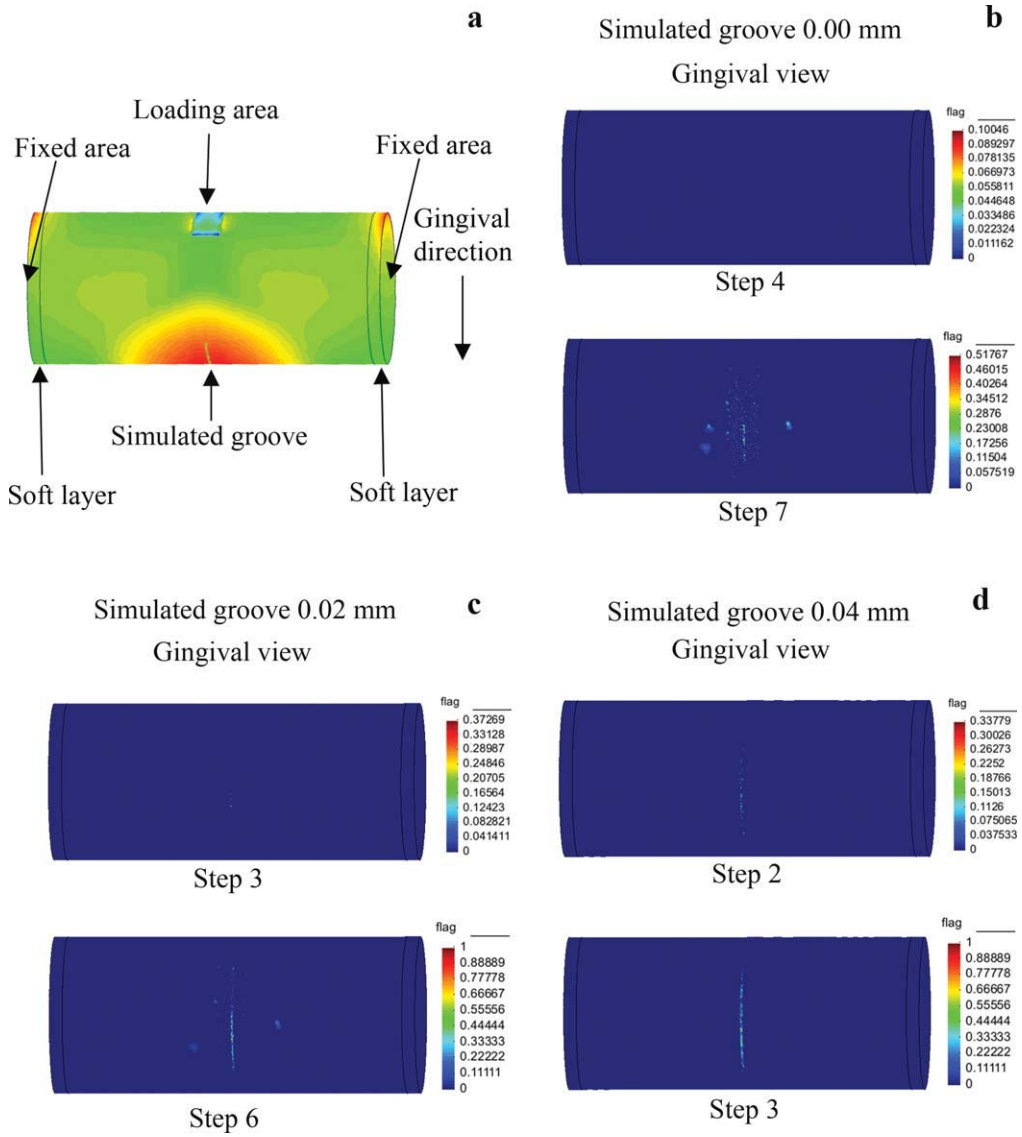

FIGURE 3. Selected steps in the fracture propagation in a cylinder-shaped bar with grooves of varying depths introduced on the surface. (a) Buccal view of the loading model. (b) Gingival view of the bar with no grooves. (c) Gingival view of the bar with a groove 0.02 mm deep. (d) Gingival view of the bar with a groove 0.04 mm deep. The color marks to the right indicate different levels of fracture. No fracture is present when the flag = 0. An element has failed completely when the flag = 1. Flag between 0 and 1 indicates that an element has partly failed. The color red indicates high flag numbers and blue indicates low flag numbers. [Color figure can be viewed in the online issue, which is available at wileyonlinelibrary.com.]

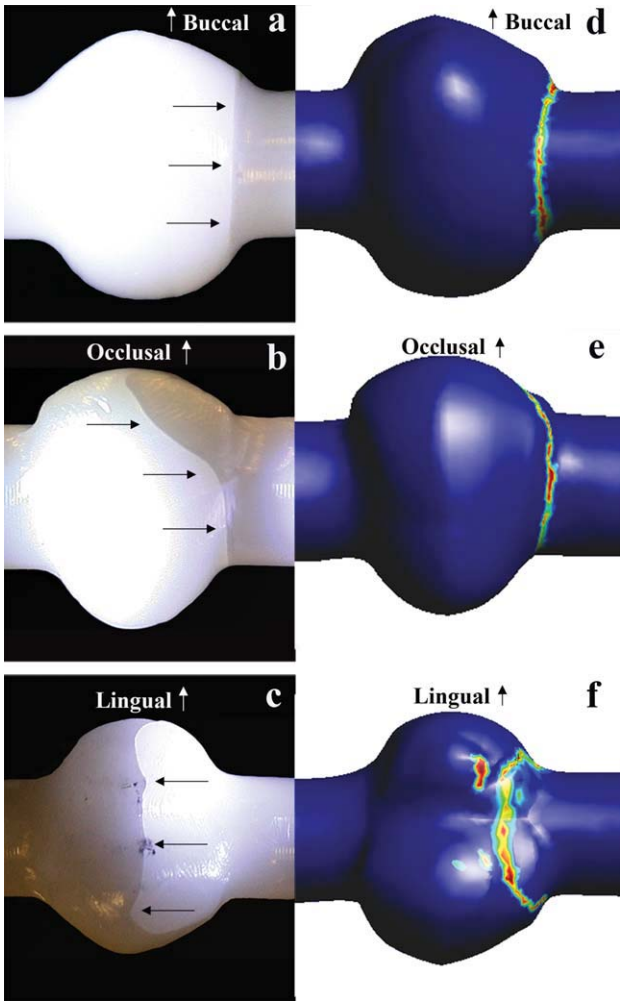

FIGURE 4. Comparison of the fracture pattern between the laboratory test and the numerical simulation. Gingival view (a,d). Buccal view (b,e). Occlusal view (c,f). In (a–c), the color difference is caused by the low angle illumination used to accentuate the fracture. The fracture is marked with black arrows. [Color figure can be viewed in the online issue, which is available at wileyonlinelibrary.com.]

areas with soft layers were created [Figure 3(a)]. The distance between these areas corresponded to the distance between the medial borders of the two framework retainers in the laboratory test. The diameter of the cylinder-shaped ceramic bar was based on the occlusal-gingival distance of the pontic of the framework in the laboratory test. The width and depths of the milling trace lines of the machined framework in the laboratory test were measured using a measuring microscope (Leitz UWM-Dig-S, Ernst Leitz GmbH, Wetzlar, Germany) at 20× magnification. The average width was 0.10 ± 0.008 mm and the average depth 0.02 ± 0.006 mm. The width and depth of a simulated groove was based on the measurements of the machined framework in the laboratory test [Figure 3(c)]. In addition, for comparison purposes, the cylinder-shaped bar was also loaded without any simulated groove [Figure 3(b)] and with a simulated groove 0.10 mm wide and 0.04 mm deep [Figure 3(d)]. In the numerical simulation, a total of 198,655 tetrahedral elements without mid-side nodes were generated.

RESULTS

Laboratory results

Figures 4(a–c) show images of the fracture patterns of the fractured framework specimen. In the gingival view the fracture ran along a groove [Figure 4(a)]. On the buccal side of the framework the fracture went between the gingival side of the framework and the loading area [Figure 4(b)]. A typical compression curl was seen in the occlusal and buccal views [Figures 4(b,c)].

Numerical simulation results

Stress distribution and fracture process. In Figures 5(a1-a3), selected steps in the maximum principal stress (σ_1) distribution are presented. The corresponding steps in the minimum principal stress (σ_3) distribution are presented in Figures 5(b1–b3). In Figure 6, selected steps in the fracture process are presented and the fracture initiation and propagation of the simulated framework are shown.

At step 3, the red and yellow areas in the gingival part of the framework indicate high tensile stress concentrations [Figure 5(a1)]. In Figure 5(b1), the blue areas indicate high levels of compressive stress in the loading areas, which is the cause of the fracture initiation seen on the occlusal part of the framework in the loading area at step 3 in Figure 6.

At step 5, the highest σ_1 value in the whole fracture process, 632.71 MPa, was reached. The location of this value was in the gingival boundary of the framework [Figure 5(a2)]. The red and yellow area on the right indicates higher tensile stress concentration than on the left side of the pontic [Figure 5(a2)], the fracture, therefore, began on the right side. This is confirmed by the initiation site on the buccal side, close to the right of the pontic in the gingival part of the framework at step 5 in Figure 6. At the loading area, the highest σ_1 value was −508.43 MPa [Figure 5(a2)] and the lowest σ_3 value was −1974.2 MPa [Figure 5(b2)]. That is, all the normal stresses in various directions in this area fell within these two values. As mentioned earlier, compressive stress is defined as a negative value in the present study. Since these values were negative, they indicate that the elements in this area were fractured by compression.

At step 6, total fracture of the simulated framework occurred in one step, an indication of brittle fracture (Figure 6, step 6). At step 18, the stress concentration in the gingival boundary disappears as the framework has already fractured [Figure 5(A3)], whereas a high σ_1 concentration was located at the occlusal part at the connector area close to the left abutment [Figure 5(A3)]. This could be the cause of the fracture initiation at the area close to the left abutment of the framework in step 18 in Figure 6.

Stress versus loading displacement in two selected nodes step by step. The software makes it possible to pick out a specific node and to follow the stress distribution step by step for that node. Figure 7 demonstrates the stress-loading displacement relationships at two selected nodes. The nodes selected are node No. 10985, located at the fractured area in the gingival boundary of the right connector on the buccal side of the framework, and node No. 49737, located at

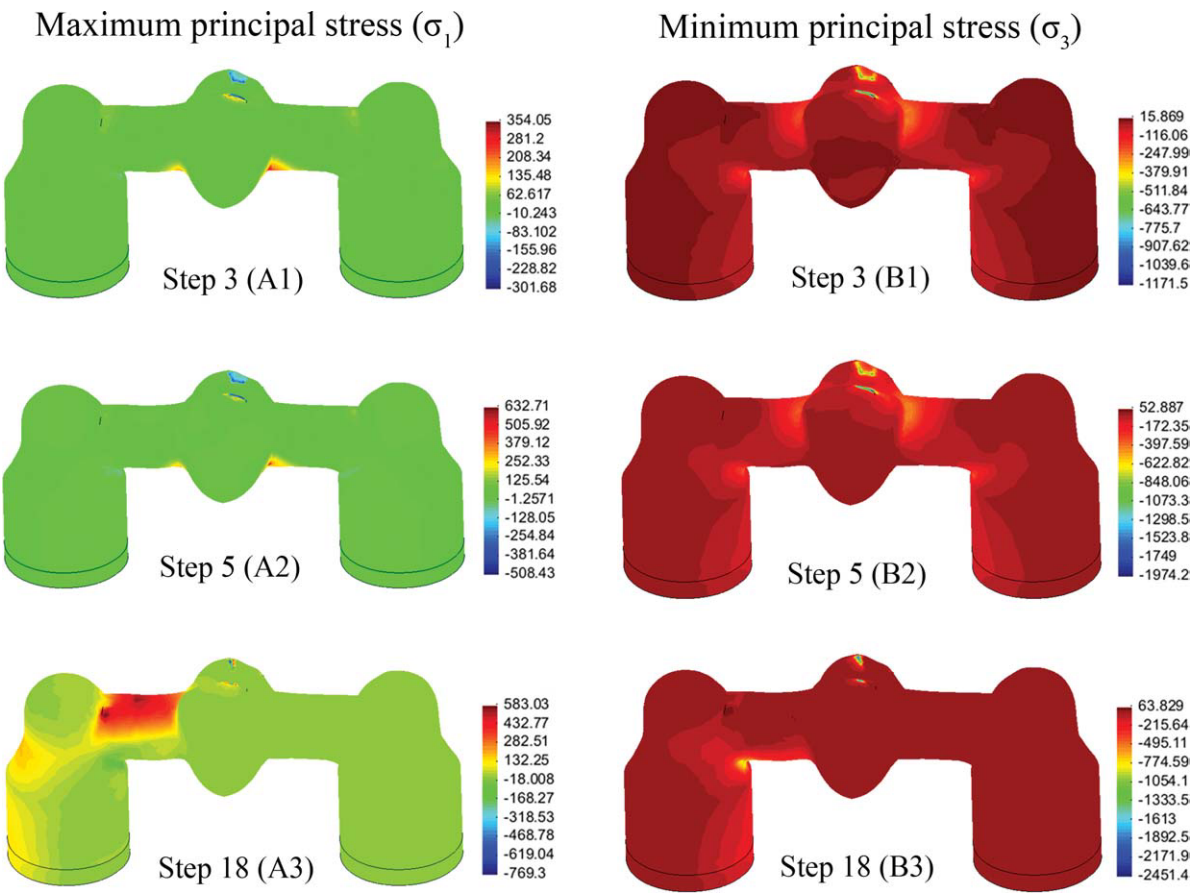

FIGURE 5. Representative views of the maximum principal stress (σ_1) distribution and minimum principal stress (σ_3) distribution. The rainbow colored marker indicates the stress value (MPa) in the three-unit framework for each step. The reddest color indicates the highest stress and the bluest color indicates the lowest stress. Tensile stress is defined with a positive value and compressive stress is defined with a negative value. Therefore, maximum principal stress (σ_1) describes the tensile stress and minimum principal stress (σ_3) describes the compressive stress. [Color figure can be viewed in the online issue, which is available at wileyonlinelibrary.com.]

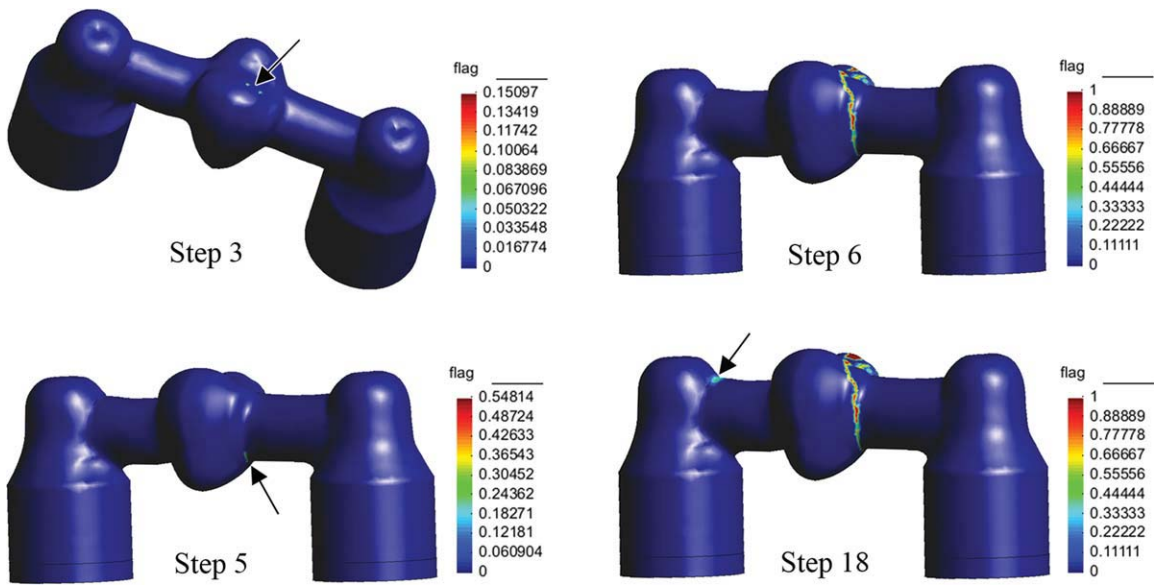

FIGURE 6. The fracture propagation in the three-unit framework. The color mark indicates different levels of fracture for each step. No fracture is present when the flag = 0. An element has completely failed when the flag = 1. Flag between 0 and 1 indicates that an element has partly failed. The color red indicates high flag numbers and blue indicates low flag numbers. [Color figure can be viewed in the online issue, which is available at wileyonlinelibrary.com.]

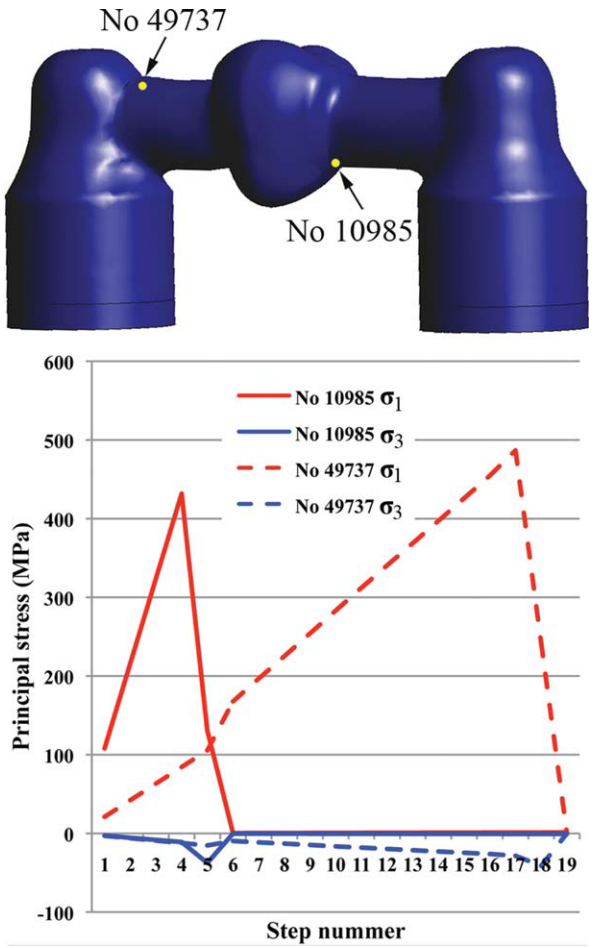

FIGURE 7. The maximum (σ_1) and minimum principal stress (σ_3) values step by step at two selected nodes of the three-unit framework. Red lines indicate maximum principal stress (σ_1) and blue lines indicate minimum principal stress (σ_3) at the selected nodes. [Color figure can be viewed in the online issue, which is available at wileyonlinelibrary.com.]

the fracture area in the upper part of the framework close to the left abutment (Figure 7). For these nodes, σ_1 and σ_3 were registered step-by-step (Figure 7).

For node No. 10985, an increase in σ_1 could be observed from step 1 to step 4 while step 5 showed a sudden decrease. Correspondingly, σ_3 showed a minor decrease at this node while from step 6 to step 19, σ_1 and σ_3 were $\sim$0 MPa (Figure 7).

For node No. 49737, a linear increase in σ_1 could be observed from step 1 to step 5 with a corresponding linear decrease of σ_3. From step 5 to step 6, a suddenly steeper increase was observed both for σ_1 and σ_3. From step 6 to step 17 a linear increase of σ_1 could be seen, and a corresponding linear decrease of σ_3. At step 18, a sudden decrease in σ_1 and σ_3 was observed. Finally, at step 19 σ_1 and σ_3 were $\sim$0 MPa (Figure 7).

Simulated grooves. The results after introducing surface grooves of various depths are presented in Figure 3. At a depth of 0.00 mm [Figure 3(b)], that is without grooves, the highest flag value was 0 before step 4, indicating that no fracture was initiated before this step. At step 4, the highest flag value was 0.10046 indicating that some elements were partly fractured. At step 7, the highest flag value was 0.51767, indicating that none of the elements had completely fractured. With a groove depth of 0.02 mm [Figure 3(c)], fracture was initiated at step 3 (flag = 0.37269) and total fracture of at least one element could be seen at step 6 (flag = 1). With a groove depth of 0.04 mm [Figure 3(d)], fracture was initiated at step 2 (flag = 0.33779) and at least one element had totally fractured by step 3 (flag = 1). Thus, the deeper the groove the sooner the bar fractured.

DISCUSSION

Experimental set-up

Usually all-ceramic FPDs consist of two layers, a ceramic framework made of a reinforced ceramic and a layer of veneer made of feldspar or glass ceramics. Since the framework is the key part that sustains the load in all-ceramic FPDs, the fracture was studied in the framework alone in the current study. In the present numerical simulation of the framework, the mechanical loading condition was static and localized to the middle of the pontic, axially at the center of the pontic in order to mimic, as far as possible, the laboratory test. However, in the oral cavity loading conditions vary among individuals and within the same individual and fatigue loading might be present. Therefore, the performance of further numerical studies involving these factors is planned using different loading conditions.

Simplifications of the abutments were made when converting the laboratory test into the numerical simulation model. In the 3D simulation it was difficult to simulate accurately the space filled with cement between the abutment and the retainer. Since the stainless steel abutments and the retainers never fractured before the fracture of the framework in laboratory tests,[16,30,32] a model with zirconia-based abutments with soft-layers at the bottom was used. Soft layers were created under the zirconia abutments to compensate for the load on them and to avoid fracture of the abutments. In addition, high values for compressive and tensile strength were chosen for the soft layers, as they should remain intact during the loading process.

Numerical modeling

Material properties. Ceramics are fairly homogeneous materials, but often contain flaws that are volumetrically distributed. Theses flaws, in the form of defects or hard inclusions, could influence the stress distribution in the material and induce further fracture initiation and propagation.[13] In the present study, the Weibull statistical method was used to describe the heterogeneity in the materials studied. Earlier studies[26] have shown the Weibull distribution method to be a satisfactory tool for describing the distribution of the defects in brittle materials such as rocks.

The Weibull modulus m in Eq. (1) is a homogeneous index of the material and ranges from 0 to infinity. When $m = 10$, as in the present study, the distribution of macroscopic parameters (compressive strength, tensile strength, or Young's modulus) are located in a narrow area close to the mean value, $\sigma_{0,}$ meaning that the material is rather homogeneous. The Weibull function provides a nonsymmetrical distribution against σ_0, indicating a greater probability of smaller values for strength and Young's modulus. Therefore, to achieve reasonable macroscopic values for strength and Young's modulus, larger values than the mean values of these parameters should be chosen. The relationship between the macroscopic parameters of the specimen and seed parameters (i.e., Weibull modulus, mean value of compressive strength/ tensile strength/ Young's modulus) of the specimen of mesoscopic elements can be described by an empirical formula.[26] However, the main focus in the present study was on the fracture pattern and the fracture process of the framework and not on the actual outcome of the stress value. Therefore, a larger value than the mean values of strength and Young's modulus was not chosen. This is part of the reason the highest maximum principal stress received from the numerical simulation to fracture of the framework was 632.71 MPa [Figure 5(a2)], which corresponds quite well with the results presented by Dittmer et al.,[19] although the tensile strength of the Y-TZP was 840 MPa (Table I). If larger values for the strengths had been selected for the simulation, the ceramic framework should have sustained higher loading. Since the normal range of Poisson's ratio in elastic materials is between 0 and 0.5, Possion's ratio did not follow the Weibull distribution law in the present study.

Failure criterion. The Mohr-Coulomb strength failure criterion with tensile strength cut-off was applied in the current study to judge whether the ceramic material was in an elastic state or had failed. A number of earlier studies addressing the fracture processes in dental ceramics used the von Mises stress.[31,33] In those studies, a higher von Mises stress indicates a greater risk of failure, but there is often no threshold stress value indicating the fracture presented in the studies. However, the intention of the von Mises failure criterion is to predict the yielding of materials under loading condition by using only the parameter shear stress and it is part of plasticity theory[34] that is best applied to ductile materials, such as metals. In the case of fracture in brittle materials, in addition to shear stress, confining stress and tensile stress also play important rolls, as has been confirmed in earlier laboratory studies.[27] Since the Mohr-Coulomb failure criterion considers the shear stress, the confining stress and the tensile stress, it was selected for use in the present study.

When the confining stress is very high, the Mohr-Coulomb failure criterion with a cap-model[26] should be used to judge fracture in brittle materials, because the material would be unable to sustain a too high confining pressure, even with very small shear stress. Similarly, tensile strength cut-off was also applied as the tensile stress could not be higher than the tensile strength of brittle material. In the present study, as the confining stress was not too high, only the Mohr-Coulomb criterion with tensile strength cut-off was applied as the failure threshold.

Comparison between the laboratory test and the numerical modeling method. The present numerical modeling provided neat results. However, it is important to assess the correctness of the outcomes and validate the simulated numerical results using laboratory studies. For validation, the fracture pattern obtained from the numerical modeling was therefore compared with the laboratory test (Figure 4). Comparison between the present numerical study and the laboratory test reveals that in the gingival part, the numerical modeling gives a fracture pattern which correlated well with the laboratory test [Figure 4(a,d)]. In the buccal part, a compression curl was seen both in the laboratory test and in the numerical simulation [Figure 4(b,e)]. A compression curl is a telltale feature of flexural fracture which indicates that the crack has started and grown perpendicularly to the tensile surface of the framework loaded in bending.[13] When the crack reached the compressive side of the framework a curved lip was formed just before the fracture was completed.[13] The compression curl indicates that the fracture started on the tensile side,[13] that is, the gingival side of the current framework. In the buccal and the occlusal parts, however, the shapes of the fracture pattern differed a little between the laboratory test and the numerical modeling [Figure 4(b,c,e,f)]. The reason for this could be the complicated loading conditions and the complex anatomy of the cusps at the occlusal surface. However, the results obtained from the numerical modeling overall provided good guidance concerning the shape of the fracture pattern of the ceramic framework, largely correlating with the laboratory test.

In addition, the fracture process obtained in the present numerical simulation was also validated by the fractographic analysis[16] performed earlier on fractured frameworks of similar material and dimensions as those in the current study. In this fractographic analysis,[16] fracture initiation sites were detected both on the occlusal part and in the gingival part of the fractured framework specimens. The location of these fracture initiation sites was similar to the findings in the present numerical modeling. Both in the numerical simulation and the fractographic analysis,[16] the location of the fracture initiation that caused the final catastrophic failure was identified as being in the right gingival portion of the framework and the main fracture mechanism for the ceramic framework was tensile failure. Although the fracture initiation sites could be localized in the fractographic analysis,[16] the fracture process could not be followed step by step. With the present numerical modeling, however, the whole fracture process could be followed step by step and the first initial fracture site in the framework was revealed on the buccal cusp in the occlusal area (Figure 6, step 3), information that could not be gained from the fractographic analysis. In the previous 2D numerical simulation[20] that considered the materials' heterogeneity, the stress distribution and the

whole fracture process could also be followed step-by-step in a simulated three-unit ceramic FPD framework. However, in contrast to the present 3D simulation the 2D simulation[20] deviated from reality to a great extent, because in the 2D simulation an infinite thickness of the framework was assumed and the localization of the fracture initiation sites could not be clearly identified.

Influence of the grooves. Milling trace lines/grooves have been observed on the surface of machined ceramic frameworks[16,21] and it has been shown that grinding ceramic core materials with diamond burs introduced irregularities on the surface.[22] To evaluate the effect on fracture of such defects on the ceramic surfaces, a numerical model of a ceramic cylinder-shaped bar was created and the influence of surface grooves of varying depths on the fracture of the ceramic bar was then studied (Figure 3). The results indicated that surface irregularities could affect the fracture, which is in agreement with an earlier fractographic analysis.[16]

Based on the findings in the present study, the 3D numerical simulation code used seems to be able to simulate fracture in ceramic frameworks both with and without introduced surface irregularities. Therefore, further validation studies of fracture processes in frameworks with varying geometric shapes, materials, loading conditions are planned. Once the simulated results received from the numerical method are assessed as sufficiently trustworthy the numerical simulation code could be used as a design tool for dental frameworks, thereby reducing the number of laboratory tests needed and reducing costs.

CONCLUSION

Within the limitations of this study the following conclusions were drawn:

1. With the newly developed 3D numerical modeling method used in the present study, the stress distribution and the fracture process in a three-unit zirconia-based FPD framework could be clearly shown and followed step by step.
2. The fracture pattern obtained from the numerical simulation largely correlated with laboratory results.
3. Similar locations for fracture initiation sites were detected both in the numerical simulation and in an earlier fractographic analysis. The first initial fracture site on the simulated framework was revealed as being the occlusal area.
4. Simulation of milling grooves in the high tensile stress concentrated area in a zirconia-based bar revealed that the deeper the groove the sooner the bar fractured.
5. Based on the above findings, the 3D numerical modeling method used in the present study seems to be a suitable tool for predicting the fracture process in ceramic FPD frameworks.

REFERENCES

1. Jones DW. Development of dental ceramics. An historical perspective. Dent Clin North Am 1985;29:621–644.
2. Ghazal M, Steiner M, Kern M. Wear resistance of artificial denture teeth. Int J Prosthodont 2008;21:166–168.
3. Denry I, Kelly JR. State of the art of zirconia for dental applications. Dent Mater 2008;24:299–307.
4. Filser F, Kocher P, Weibel F, Luthy H, Scharer P, Gauckler LJ. Reliability and strength of all-ceramic dental restorations fabricated by direct ceramic machining (DCM). Int J Comput Dent 2001;4:89–106.
5. Andersson M, Odén A. A new all-ceramic crown. A dense-sintered, high-purity alumina coping with porcelain. Acta Odontol Scand 1993;51:59–64.
6. Sundh A, Sjögren G. A comparison of fracture strength of yttrium-oxide- partially-stabilized zirconia ceramic crowns with varying core thickness, shapes and veneer ceramics. J Oral Rehabil 2004;31:682–688.
7. Christel P, Meunier A, Heller M, Torre JP, Peille CN. Mechanical properties and short-term in-vivo evaluation of yttrium-oxide-partially-stabilized zirconia. J Biomed Mater Res 1989;23:45–61.
8. Hannink RHJ, Kelly PM, Muddle BC. Transformation toughning in zirconia-containing ceramics. J Am Ceram Soc 2000;83: 461–487.
9. Molin MK, Karlsson SL. Five-year clinical prospective evaluation of zirconia-based Denzir 3-unit FPDs. Int J Prosthodont 2008;21: 223–227.
10. Tinschert J, Schulze KA, Natt G, Latzke P, Heussen N, Spiekermann H. Clinical behavior of zirconia-based fixed partial dentures made of DC-Zirkon: 3-Year results. Int J Prosthodont 2008;21: 217–222.
11. Sailer I, Feher A, Filser F, Gauckler LJ, Luthy H, Hammerle CH. Five-year clinical results of zirconia frameworks for posterior fixed partial dentures. Int J Prosthodont 2007;20:383–388.
12. Roediger M, Gersdorff N, Huels A, Rinke S. Prospective evaluation of zirconia posterior fixed partial dentures: Four-year clinical results. Int J Prosthodont 2010;23:141–148.
13. Quinn GD. NIST Recommended Practice Guide: Fractography of Ceramics and Glasses. Washington, DC: National Institute of Standards and Technology; 2007.
14. Quinn JB, Quinn GD, Kelly JR, Scherrer SS. Fractographic analyses of three ceramic whole crown restoration failures. Dent Mater 2005;21:920–929.
15. Scherrer SS, Quinn GD, Quinn JB. Fractographic failure analysis of a Procera AllCeram crown using stereo and scanning electron microscopy. Dent Mater 2008;24:1107–1113.
16. Kou W, Sjögren G. Fracture behaviour of zirconia FPDs substructures. J Oral Rehabil 2010;37:292–299.
17. Oruc S, Eraslan O, Tukay HA, Atay A. Stress analysis of effects of nonrigid connectors on fixed partial dentures with pier abutments. J Prosthet Dent 2008;99:185–192.
18. Tanaka E, Koolstra JH. Biomechanics of the temporomandibular joint. J Dent Res 2008;87:989–991.
19. Dittmer MP, Kohorst P, Borchers L, Stiesch-Scholz M. Finite element analysis of a four-unit all-ceramic fixed partial denture. Acta Biomater 2009;5:1349–1355.
20. Kou W, Kou SQ, Liu HY, Sjögren G. Numerical modeling of the fracture process in a three-unit all-ceramic fixed partial denture. Dent Mater 2007;23:1042–1049.
21. Aboushelib MN, Feilzer AJ, Kleverlaan CJ. Bridging the gap between clinical failure and laboratory fracture strength tests using a fractographic approach. Dent Mater 2009;25:383– 391.
22. Kou W, Molin M, Sjögren G. Surface roughness of five different dental ceramic core materials after grinding and polishing. J Oral Rehabil 2006;33:117–124.
23. Oh W, Gotzen N, Anusavice KJ. Influence of connector design on fracture probability of ceramic fixed-partial dentures. J Dent Res 2002;81:623–627.
24. Oh WS, Anusavice KJ. Effect of connector design on the fracture resistance of all-ceramic fixed partial dentures. J Prosthet Dent 2002;87:536–542.
25. Weibull W. A statistical distribution function of wide applicability. J Appl Mech 1951;18:293–297.
26. Liu HY. Numerical Modeling of the Rock Fragmentation Process by Mechanical Tools. Doctoral Thesis. Luleå, Sweden: Luleå University of Technology; 2004.
27. Jaeger JC, Cook NGW. Fundamentals of rock mechanics. London: Chapman and Hall, Ltd; 1976.

28. Guazzato M, Albakry M, Ringer SP, Swain MV. Strength, fracture toughness and microstructure of a selection of all-ceramic materials. Part II. Zirconia-based dental ceramics. Dent Mater 2004;20:449–56.
29. Guazzato M, Quach L, Albakry M, Swain MV. Influence of surface and heat treatments on the flexural strength of Y-TZP dental ceramic. J Dent 2005;33:9–18.
30. Sundh A, Sjögren G. Fracture resistance of all-ceramic zirconia bridges with differing phase stabilizers and quality of sintering. Dent Mater 2006;22:778–784.
31. Eraslan O, Sevimay M, Usumez A, Eskitascioglu G. Effects of cantilever design and material on stress distribution in fixed partial dentures—A finite element analysis. J Oral Rehabil 2005; 32:273–278.
32. Sundh A, Molin M, Sjögren G. Fracture resistance of yttrium oxide partially-stabilized zirconia all-ceramic bridges after veneering and mechanical fatigue testing. Dent Mater 2005;21: 476–482.
33. Tsumita M, Kokubo Y, Vult von Steyern P, Fukushima S. Effect of framework shape on the fracture strength of implant-supported all-ceramic fixed partial dentures in the molar region. J Prosthodont 2008;17:274–285.
34. Von Mises R. Mechanik der festen korper im plastisch deformablen zustand. Göttin Nachr Math Phys 1913;1:582–592.